

https://doi.org/10.1070/QEL16901

Confocal Raman imaging of skin sections containing hair follicles using classical least squares regression and multivariate curve resolution–alternating least squares

J. Schleusener*, V. Carrer*, A. Patzelt, S. Guo, T. Bocklitz, L. Coderch, J. Lademann, M.E. Darvin

Abstract. **Confocal Raman microscopy (CRM) is applied *ex vivo* for imaging of the spatial distribution of different skin components in skin sections containing hair follicles. For multivariate data analysis, different methods are used in order to spectrally decompose the reference spectra of the skin components (dermis, viable epidermis, stratum corneum and hair). Classical least squares regression (CLS) and multivariate curve resolution–alternating least squares (MCR-ALS) are chosen as suitable methods. In comparison to other optical methods, the advantage of CRM is molecular specificity and dispensability of labelling dyes, which is e.g. necessary in fluorescence microscopy. Therefore, a useful future application of CRM in combination with multivariate data analysis lies in the analysis of penetration routes of topically applied substances, such as cosmetic formulations or drugs into the skin, which is particularly interesting in and around hair follicles.**

Keywords: *dermatology, optical profilometry, multivariate data analysis, hyperspectral imaging, skin imaging, confocal Raman microscopy.*

1. Introduction

Over the years, diverse optical methods for microscopic imaging of skin sections and hair follicles have been applied. Hair follicles are considered interesting because they contain a diversity of skin and hair components in close proximity and are an important route for the penetration of topically applied drugs [1, 2]. Anatomically, a hair follicle embodies an invagination of the epidermis resulting in an increased surface area available for absorption of drugs. Moreover, these invaginations are surrounded by numerous blood capillaries that facilitate systemic absorption of drugs. Numerous antigen presenting cells around the upper part of the hair follicles are of special interest with regard to immunological therapy. Furthermore, recent studies showed that the hair follicle can be a long-term drug reservoir for topically applied nanocarriers for a time period of up to 10 days [3].

Conventional light microscopy is a fast and simple method that is suitable for morphologic imaging and is vastly applied in histology. Confocal laser scanning microscopy (CLSM) can be used in reflectance and fluorescence modes [4, 5]. The latter also enables the visualisation of the distribution of a fluorescent dye in a biological sample. This is e.g. useful for analysis of the penetration depth of topically applied substances into the skin. Thereby, the visualisation and even the quantification of the applied substances are achieved [6, 7]. However, the penetration characteristic between applied substances and added fluorescent dyes may differ.

Several methods are also available for label free imaging of the intrinsic molecular composition of biomedical samples [8] like skin. Two-photon microscopy combined with the fluorescence lifetime imaging technique (FLIM) can be also applied for penetration studies, but the limitations are strong due to the frequent superposition between skin and substances' characteristics [9, 10]. A clear advantage of CLSM and two-photon microscopy is the rapid data acquisition time, which enables *in vivo* measurements on the skin.

Further, the application of stimulated Raman scattering (SRS) microscopy allows for label-free imaging with high spatial resolution of different chemical components and can be used to image the penetration of topically applied substances [11, 12].

IR microspectroscopy and confocal Raman microscopy (CRM) can provide molecular information and can also be employed to evaluate the permeation of topically applied agents into the skin [13–17]. Both optical techniques can combine the spectral and the spatial information in order to be used for hyperspectral imaging. While the data acquisition time is considerably slower with Raman than with CLSM using isotopically labelled functional groups, the technique allows not only for detection of the molecular composition, but also for monitoring of hydrogen bonding states of water molecules [18], structural changes (e.g. protein secondary and tertiary structures [18, 19] and lipid chain ordering [20, 21] *ex vivo* and *in vivo*, which has recently been shown for single

* These authors contributed equally to this work.

J. Schleusener, A. Patzelt, J. Lademann, M.E. Darvin Charité – Universitätsmedizin Berlin, corporate member of Freie Universität Berlin, Humboldt-Universität zu Berlin, and Berlin Institute of Health, Department of Dermatology, Venerology and Allergology, Center of Experimental and Applied Cutaneous Physiology, Charitéplatz 1, 10117 Berlin, Germany; e-mail: juergen.lademann@charite.de;
V. Carrer Charité – Universitätsmedizin Berlin, corporate member of Freie Universität Berlin, Humboldt-Universität zu Berlin, and Berlin Institute of Health, Department of Dermatology, Venerology and Allergology, Center of Experimental and Applied Cutaneous Physiology, Charitéplatz 1, 10117 Berlin, Germany; Institute of Advanced Chemistry of Catalonia, Department of Chemical and Surfactants Technology, Jordi Girona 18-26, 08034 Barcelona, Spain;
S. Guo, T. Bocklitz Institute of Physical Chemistry and Abbe Center of Photonics, Friedrich-Schiller-University of Jena, Helmholtzweg 4, 07743 Jena, Germany; Leibniz Institute of Photonic Technology, Member of Leibniz Research Alliance 'Health Technologies', Albert-Einstein-Straße 9, 07745 Jena, Germany;
L. Coderch Institute of Advanced Chemistry of Catalonia, Department of Chemical and Surfactants Technology, Jordi Girona 18-26, 08034 Barcelona, Spain

Received 25 September 2018; revision received 12 October 2018
Kvantovaya Elektronika **49** (1) 6–12 (2019)
Submitted in English

point depth profiling of the stratum corneum, and which provides information about the skin barrier function [22–24]. However, due to the slow data acquisition times of the scanning process, these methods are not ideally suitable for 3D *in vivo* imaging measurements of the skin, which could be potentially accelerated using multiplex approaches in the future [25, 26].

With CRM, the relative abundance of different biomolecules in the measurement volume can be determined based on the intensity of the Raman bands, which enables the differentiation of cells, tissues and skin and of topically applied substances. Also, the identification of tattoo pigments in case of tattooed skin was accomplished [27]. Besides the spectroscopic analysis of the individual chemical composition, CRM offers imaging possibility by scanning the sample, which therefore facilitates the visualisation of spatially resolved component distribution. Several methods have been applied for imaging of Raman spectra. For molecular imaging of the different contributions of skin components or topically applied substances as e.g. caffeine [28], at different positions use can be made of mapping of the integrated area under the curve (AUC) or the nonlinear regression of a Gaussian function of single Raman bands. However, individual bands in the Raman spectra can usually not be associated with different skin components, due to their presence in different components for varying concentration. Also, the usefulness of this method for imaging of follicular penetration might be limited, due to the potential superposition of skin-based and substance-based bands. An advantage of these methods is their simplicity, but in case of strongly superimposed components, artifacts are likely to occur, which would lead to misidentification. In order to circumvent this shortcoming and to detect very small spectral differences, several multivariate analysis methods exist, considering information about the entire Raman spectra as opposed to individual Raman bands [29].

Zhang et al. [30] used multivariate factor analysis to determine regions of similarity, which were, based on their location, subsequently assigned to skin components, such as stratum corneum, viable epidermis and dermis. Tsai et al. [31] used principal component analysis combined with linear discriminant analysis for imaging of stem cells in the hair bulge in the follicle, where their density is comparably high. This method is intended to detect differences of two classes of spectra. Based on *a priori* knowledge of the class affiliation, sensitivities and specificities of the method can be calculated. Franzen et al. [32] used a multivariate analysis method for molecular imaging on hair follicles and differentiated the contribution of hair, epidermis, dermis and sebum [2]. Thereby, similarities in sebum of human and porcine hair follicles were found, and their distribution on the hair was imaged. This is important information, because follicular sebum is a release medium for drugs penetrating through the follicular pathway. Drug delivery to hair follicles is likely dependent on the physicochemical properties of the drugs, lipidic similarity between the sebum and the formulation, as well as on the activity status, size and density of the hair follicle [33, 34].

Classical least squares regression (CLS) is another method for identification of different components. CLS requires the reference spectrum (loading) of each pure compound in the sample to calculate their contributions in the dataset (scores). This algorithm approximates the spectrum at each position as a linear combination of all the reference spectra. The scaling factors (scores), corresponding to each reference spectrum, are optimised to get the best fit of the original spectrum. The resulting scores are then used to create a map showing the distribution of the pure compounds. CLS is considered to be the most reliable method in cases where all the reference spectra of the pure compounds in the sample are known, as has been used, e.g. for the Raman based imaging of chemical substance distribution in pharmaceutical tablets [35, 36] or the penetration depth of topically applied substances [37]. The availability of reference spectra of pure substances, however, can be problematic to access when measuring biological tissues or cells with complex amounts of constituents and only a limited number of reference spectra available. With regard to skin, Caspers et al. [38] have improved the quantification by using spectra of pure substances of SC components. The efficiency of CLS is further reduced in the presence of position shifts or changes of broadness of Raman bands, which might occur if the pure substances interact with each other. One possibility to improve CLS could be the selection of specific wavelength ranges for the analysis [39].

An alternative method is multivariate curve resolution–alternating least squares (MCR-ALS) [40], which has been widely used for different applications of Raman-based hyperspectral imaging [41, 42] and investigations of substances' penetration into the skin [43]. Similar to CLS, MCR-ALS can recover the concentration and pure spectra of analytes of interest and can additionally estimate the spectra of possible interferences. This method is proved to be particularly useful in cases where spectra of the pure substances are not available [44–47]. Using MCR-ALS, e.g. the imaging of resolved components on several forms of skin cancer has been accomplished [48]. Mathematically, all spectra of the collective mixture are decomposed into two matrices: loadings and scores. The loadings are referred to as chemically interpretable basis that reflect the spectra of components; the scores represent the concentration profiles of the corresponding component. This decomposition is conducted using an iterative alternating least squares method [49–51]. The number of contributing pure components can be estimated using singular value decomposition. Unlike CLS, the pure spectra of the components do not have to be available in MCR-ALS. Instead, the pure spectra can be initially estimated with the SIMPLISMA algorithm [52]. However, available reference spectra can serve as a starting point for the iterative optimisation procedure. The main advantage of CLS and MCR-ALS is their ability to analyse the whole spectra instead of single band intensities.

In this study, we investigated the spatial distribution of skin components in hair follicle containing skin sections using Raman microscopic imaging combined with CLS and MCR-ALS models. We compared the CLS and MCR-ALS models according to their performance to extract semi-quantitative and spatially resolved information about the skin components. It was shown that skin components can be clearly distinguished based on their molecular structures revealed by their Raman spectra. This provides additional information that cannot be extracted by conventional imaging methods such as laser scanning microscopy. In addition, the results can be further improved by combining a pre-step differentiation of the different skin components. This study demonstrates the potential of Raman microscopic imaging in combination with CLS and MCR-ALS models for identifying the penetration characteristics of topically applied substances, which is challenging due to their low concentration and the multitude of native components in the skin.

2. Methods

2.1. Skin sample preparation

Porcine skin was chosen in this study due to its morphological similarity to human skin [5] and its suitability for *ex vivo* measurements [5, 53]. The Raman-spectral similarities between the human and porcine skin components have also been widely reported [9, 54]. The porcine ear was provided by a local butcher and was used for the experiments on the day of slaughter. The ear was cleaned with cold flowing water and was dried with paper towels. The bristles were carefully shortened with scissors to not affect the integrity of the stratum corneum. Biopsies were taken using a scalpel. Cryospray (Cryo-Spray, SLEE medical GmbH, Mainz, Germany) was applied to facilitate separation of the skin samples from the underlying tissue. The biopsies were flattened between two glass slides, again fixed with cryospray, placed in liquid nitrogen and subsequently stored in a freezer at −20 °C until further processing. The experiments were approved by the Veterinary and Food Inspection Office, Dahme Spreewald, Germany.

2.2. Cryohistological cross sections

The cross-sectional tissue samples of the biopsies were prepared using a cryomicrotome (Cryostat Microm HM 560, Microm International GmbH, Walldorf, Germany). Each biopsy was embedded in tissue freezing medium (Leica Biosystems Nussloch GmbH, Nussloch, Germany) on a metal sample holder inside the cryomicrotome at −30 °C. The embedded skin was sectioned into 30 µm slices by microtome blades before being placed onto superfrost glass slides (Carl Roth GmbH + Co KG, Karlsruhe, Germany) and for later analysis stored at −20 °C. For the subsequent measurements, the sections containing hair follicles were selected.

2.3. Confocal Raman microscopy

2.3.1. Mapping acquisition. Measurements of hair follicle containing skin sections were performed using a Labram HR800 Evolution CRM (Horiba Jobin Yvon, France) in the fingerprint region (FP, 400–2500 cm^{-1}) with excitation at 473 nm and 6.1 mW optical power on the sample surface, a 600 lines mm^{-1} grating and a spectral resolution of <4 cm^{-1}. The advantage of blue light for this application is a smaller spot size in comparison to infrared excitation. As measurements are only taken from the surface of the sections, the reduced light penetration depth into the skin, due to absorption and scattering [55, 56], is negligible. The microscopic images of the hair follicles were collected with a 10× objective, Raman measurements were performed with a 100× objective. The mapped areas were selected considering the extension of each hair follicle. The maps of the hair follicle included 80×90 spectra in an area of 1 mm^2. With a 5 s exposure time per spectrum, the total acquisition time for one section took several hours and was performed overnight.

The autofocus reflection mode integrated in the Labspec software (Horiba Jobin Yvon, France) was employed for the detection of the sample surface for every position, which was based on the intensity of the reflected light, instead of a Raman signal [57]. This decreased the total acquisition time, as only one spectrum was acquired for every x, y coordinate. The autofocus setup was established individually for the hair follicles according to the following procedure: by visually focusing on the sample, a z-value of 0 was assigned to the lowest point of the sample (glass cover-slide), then the z-value of the highest point of the sample was obtained (normally placed on the hair). Thereby, the setup range for the autofocus was established, which was scanned in 1 µm increments for the surface determination in the mappings.

2.3.2. Reference component spectra. Reference spectra of pure substances were used in the CLS and MCR-ALS methods to determine the distribution of the compound in the hair follicle. Reference spectra of stratum corneum (SC), viable epidermis, dermis, hair, glass substrate and cryospray drops were obtained from unambiguously assignable positions of a cryo-section that was only used for this purpose.

Except for a five times longer integration time, all reference measurements were performed on the same settings, as employed for the mapping acquisition.

2.4. CLS and MCR-ALS data analysis

2.4.1. CLS. The CLS fitting was performed with the Labspec software. Cosmic spikes were removed and the fluorescence background was fitted with a seventh order polynomial and subtracted from the Raman spectra. Subsequently, multivariate CLS regression was performed using the reference component spectra. The contributions were normalised in order to let the sum of scores be 100%, and were restricted to non-negativity. Finally, all contributions of the different components were plotted in false colour intensity images in relation to the microscopic images. As each Raman spectrum is a fingerprint of the chemical composition of the sample, the spatial distribution of different substances can be analysed. By assigning each component to a colour, the distribution of all reference spectra within the examined section can be indicated giving a colour-coded image of the scanned area. Mixtures of substances appear in mixed colours.

2.4.2. MCR-ALS. The recorded spectra were also analysed using the MCR-ALS algorithm. This was performed using in-house written algorithms based on the programming language Gnu R [58]. All spectra were pre-processed including spike removal, baseline correction, and vector normalisation [59, 60]. In particular, the baseline correction was achieved with the asymmetric least squares (ALS) approach in the 'baseline' package [61]. The MCR-ALS was conducted using the 'ALS' package [62]. Reference spectra of the components were applied as initial estimates of MCR-ALS. The only constraint applied for the optimisation process was non-negativity of the resolved scores and loadings [63]. The score of each component was divided by the sum of all scores for every measured position in order to obtain the semi-quantitative parameters of the corresponding component, as was done by Vajna et al. [36].

3. Results and discussion

3.1. Reference component spectra

Figure 1 shows the pre-processed spectra of the hair follicle components and external components, respectively. Noticeable differences between the tissue spectra (SC, hair, viable epidermis and dermis) can be observed. A major difference recognised in the hair spectrum is the sulphur content [64], which is indicated by the relatively higher intensities of the S–S-related band around 510–530 cm^{-1} [65]. The higher

amount of sulphur is due to the higher amounts of sulphur-containing amino acids (cysteine) from the hair's hard keratins. In the hair, 7%–8% of the amino acids are cysteine, whereas in the SC (another highly keratinised tissue) it represents only 0.5% [66]. The higher content of keratin in the hair is also indicated by the higher amide I band at 1650 cm^{-1} compared to the other spectra.

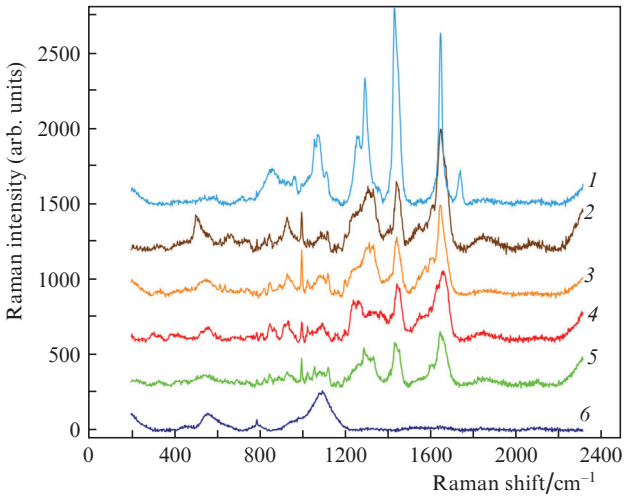

Figure 1. (Colour online) Reference Raman spectra of (*1*) cryospray, (*2*) hair, (*3*) viable epidermis, (*4*) dermis, (*5*) stratum corneum and (*6*) glass substrate in the fingerprint region. For clarity, the spectra are shown offset.

The SC shows some particularities compared to the hair, not only on the lower intensities of the bands related to the sulphur content previously detected (505 and 1650 cm^{-1}), but also for the presence of a prominent band at 1064 cm^{-1} related to the skeletal C–C stretch of lipids [67].

The dermis spectrum can be differentiated from that of the epidermis by the two double bands in the 815–850 cm^{-1} and 920–940 cm^{-1} ranges. This pattern is typical of collagen [68], which is localised in the papillary and reticular dermis [69–71], and is sensitive to collagen hydration [72]. On the other hand, the amide I band associated to proteins (1650 cm^{-1}) is highest for the hair spectrum, which is due to the higher keratin content in hair.

3.2. Mapping results

3.2.2. CLS. After processing the spectral data with CLS to identify the component distribution, a false colour Raman image is obtained, with the colours representing the contribution of the reference Raman spectra from the fingerprint range. A microscopic overview image, stitched from two photographic images, of a skin section containing a hair follicle with an intact hair, which was used for the Raman analysis, is shown in Fig. 2a. In Fig. 2b, the dermis is shown in red, viable epidermis in yellow, hair in brown, SC in green, cover-slide glass in navy blue and cryospray drops in light blue. This approach displays differences in intensity scores and allows the spatial association of multiple components simultaneously in one position. Therefore, a detailed depiction of the distribution of the different components is provided.

In Fig. 2b, the hair is correctly assigned in the cryosections. The viable epidermis and the dermis can be clearly differentiated in two different layers. The distributions of the three compounds (hair, viable epidermis and dermis) fit the distribution in the microscopic image when compared side by side. Correctly mapping the distribution of the SC is more challenging; the obtained scores are distributed not only on the skin surface, but also scattered on the hair and on the deepest region of the hair follicle. The SC is correctly marked in the infundibulum and external SC, where it has a thickness of 10–20 μm [73]. Below the infundibulum, the scores of the SC are rather discontinuous and less intense in the cryo-sections. One possible explanation could be that whereas in the upper infundibulum the epithelium is covered by intact SC, the barrier of the lower infundibulum is interrupted as the differential pattern switches from epidermal to tricholemmal differentiation [74]. Therefore, the collected spectra in these regions are gradually changing to more 'epidermis-like' features. The SC scores are also plotted broadly nearby the cryospray drops, in the deeper area of the mapped area. It should be remarked, that in this area also other components are not well allocated. The scores of hair, SC and glass are mapped in this region but none of these components are observed nearby in the microscopic image. Therefore, we suggest that the cryo-

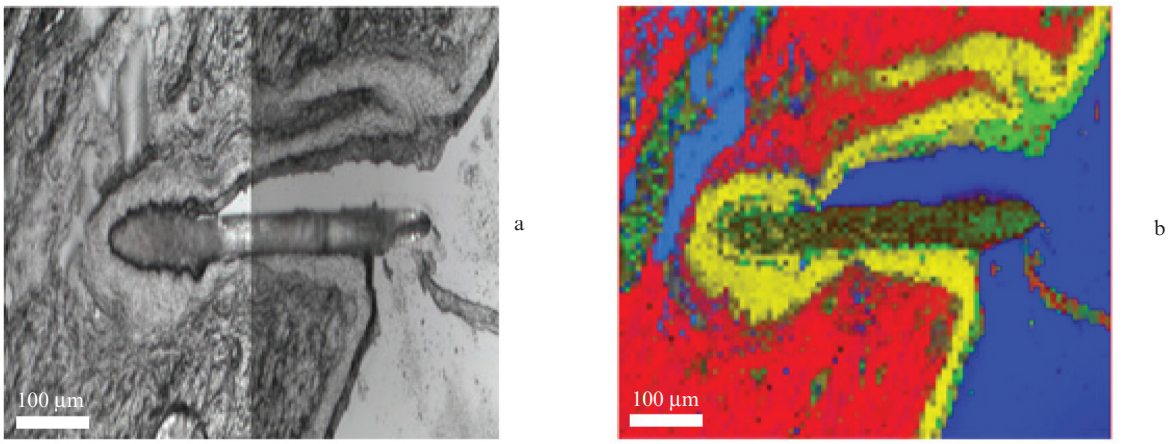

Figure 2. (Colour online) (a) Microscopic overview image of a skin section containing a hair follicle with an intact hair, stitched from two photographic images, and (b) CLS scores of Raman spectra for the same hair follicle.

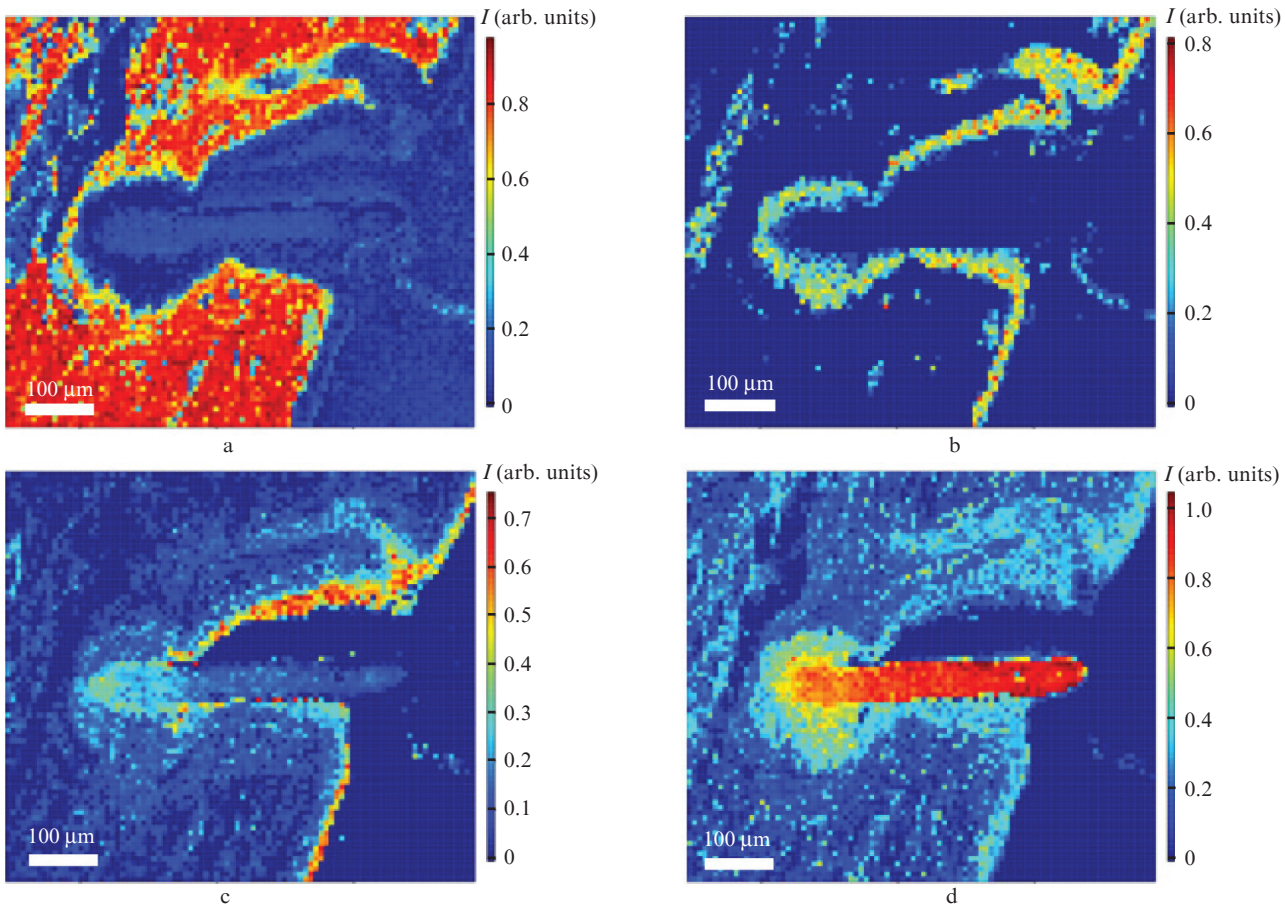

Figure 3. (Colour online) Heat maps of MCR-ALS scores of (a) dermis (a), (b) viable epidermis, (c) stratum corneum and (d) hair in relation to the position on the hair follicle.

spray drops may interfere with the measurements, clogging up the correct component identification in this area. The elongated region on the right of the hair located on the glass substrate shows residuals from the cryo-sectioning process and exposes contribution of various components.

3.2.3. MCR-ALS. The same hair follicles were also analysed with MCR-ALS. The resulting scores are plotted in heat maps in relation to their respective acquired microscopic images shown in Fig. 2a. The Raman spectra of dermis, viable epidermis, SC, hair, glass substrate and cryospray drops were employed as starting estimates for the calculations.

Figure 3 shows the heat maps of scores for the intrinsic components dermis, viable epidermis, stratum corneum and hair. The extrinsic components glass and cryospray are shown in Fig. 4. The dermis, SC and hair regions are correctly identified. In the latter case, the surrounding areas in the lowest part of the hair follicle also show considerable contribution of the hair. Due to spectral similarity between

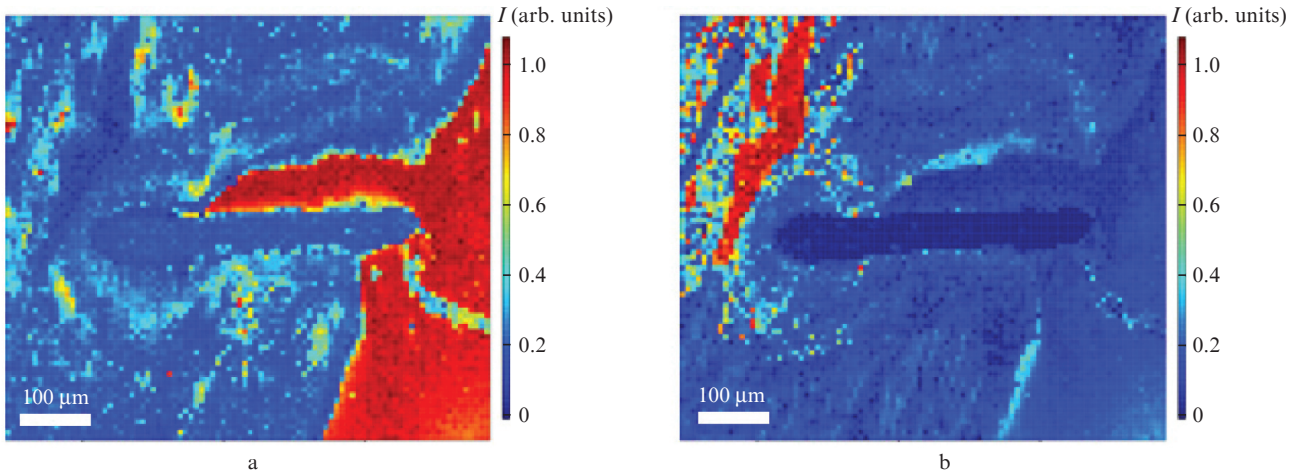

Figure 4. (Colour online) Heat maps of MCR-ALS scores of (a) glass substrate and (b) cryospray in relation to the position on the hair follicle.

hair and epidermis components, the epidermal regions also show some contribution of the hair component, which is smaller by a factor of ~2. The SC is mostly assigned correctly but shows some artifacts in the regions below the hair follicle, which is mostly identified as cryospray, as shown in Fig. 4b. The cryospray drops and the glass substrate is most distinctly identified. This can be explained by the pronounced spectral differences.

4. Conclusions

Skin sections containing hair follicles have been analysed by CRM. The analysis was based on multivariate data analysis for detection of the spatial distribution of the skin components (SC, viable epidermis, dermis and hair).

The CLS method maps the distribution of the selected components reasonably good. Some interference was observed when cryospray drops were detected but the main structures of the hair follicle were correctly displayed. Therefore, the spatial distribution of skin structures is possible with this method. The results obtained by MCR-ALS showed similar distribution of the components in the follicles to the obtained results using CLS.

We can conclude that confocal Raman microscopy combined with the CLS or the MCR-ALS data analysis enables visualisation and characterisation of the follicle's most important components without any labelling or staining. Furthermore, the methodology bares a high potential to track penetration of drugs and drug delivery systems via the follicular or transfollicular pathway. For accurate determination of the distribution of topically applied substances, more sophisticated discriminant analysis methods appear promising. For these methods, however, training sets with a known substance distribution is necessary. This is also an important step in order to validate the applied methods. The long-term immersion of skin sections in substances, with assumed homogenous distribution, could be one approach to achieve this task.

Acknowledgements. Co-author Victor Carrer made a significant contribution to this paper. He died of a tragic traffic accident in July 2018. We will always keep him in our memory.

The authors report no conflict of interest.

References

1. Radtke M., Patzelt A., Knorr F., Lademann J., Netz R.R. *Eur. J. Pharm. Biopharm.*, **116**, 1251 (2017).
2. Abd E., Benson H.A.E., Roberts M.S., Grice J.E. *Skin Pharmacol. Physiol.*, **31**, 252 (2018).
3. Lademann J., Richter H., Schaefer U.F., Blume-Peytavi U., Teichmann A., Otberg N., Sterry W. *Skin Pharmacol. Physiol.*, **19**, 232 (2006).
4. Ossadnik K., Philipp S., Bost W., Fournelle M., Richter H., Lademann J. *Skin Pharmacol. Physiol.*, **31**, 308 (2018).
5. Darvin M.E., Richter H., Zhu Y.J., Meinke M.C., Knorr F., Gonchukov S.A., Koeenig K., Lademann J. *Quantum Electron.*, **44**, 646 (2014) [*Kvantovaya Elektron.*, **44**, 646 (2014)].
6. Grams Y.Y., Whitehead L., Cornwell P., Bouwstra J.A. *Pharmaceutical Res.*, **21**, 851 (2004).
7. Grams Y.Y., Whitehead L., Cornwell P., Bouwstra J.A. *J. Controlled Release*, **98**, 367 (2004).
8. Vogler N., Meyer T., Akimov D., Latka I., Krafft C., Bendsoe N., Svanberg K., Dietzek B., Popp J. *J. Biophotonics*, **3**, 728 (2010).
9. Zhu Y., Choe C.S., Ahlberg S., Meinke M.C., Alexiev U., Lademann J., Darvin M.E. *J. Biomed. Opt.*, **20**, 051006 (2015).
10. Darvin M.E., Konig K., Kellner-Hoefer M., Breunig H.G., Werncke W., Meinke M.C., Patzelt A., Sterry W., Lademann J. *Skin Pharmacol. Physiol.*, **25**, 219 (2012).
11. Saar B.G., Contreras-Rojas L.R., Xie X.S., Guy R.H. *Mol. Pharmaceutics*, **8**, 969 (2011).
12. Giulbudagian M., Rancan F., Klossek A., Yamamoto K., Jurisch J., Neto V.C., Schrade P., Bachmann S., Ruhl E., Blume-Peytavi U., Vogt A., Calderon M. *J. Controlled Release*, **243**, 323 (2016).
13. Lasch P., Pacifico A., Diem M. *Biopolymers*, **67**, 335 (2002).
14. Cotte M., Dumas P., Besnard M., Tchoreloff P., Walter P. *J. Controlled Release*, **97**, 269 (2004).
15. Mendelsohn R., Flach C.R., Moore D.J. *Biochim. Biophys. Acta*, **1758**, 923 (2006).
16. Mujica Ascencio S., Choe C., Meinke M.C., Muller R.H., Maksimov G.V., Wigger-Alberti W., Lademann J., Darvin M.E. *Eur. J. Pharmaceut. Biopharmaceut.*, **104**, 51 (2016).
17. Souza C., Maia Campos P., Schanzer S., Albrecht S., Lohan S.B., Lademann J., Darvin M.E., Meinke M.C. *Skin Pharmacol. Physiol.*, **30**, 81 (2017).
18. Choe C., Lademann J., Darvin M.E. *Analyst*, **141**, 6329 (2016).
19. Choe C., Schleusener J., Lademann J., Darvin M.E. *Sci. Rep.*, **7**, 15900 (2017).
20. Choe C., Lademann J., Darvin M.E. *Analyst*, **141**, 1981 (2016).
21. Vyumvuhore R., Tfayli A., Duplan H., Delalleau A., Manfait M., Baillet-Guffroy A. **138**, 4103 (2013).
22. Richters R.J.H., Falcone D., Uzunbajakava N.E., Varghese B., Caspers P.J., Puppels G.J., van Erp P.E.J., van de Kerkhof P.C.M. *Skin Pharmacol. Physiol.*, **30**, 1 (2017).
23. Choe C., Schleusener J., Lademann J., Darvin M.E. *J. Biophotonics*, **11**, e201700355 (2018).
24. Choe C., Schleusener J., Lademann J., Darvin M.E. *Mech. Ageing Dev.*, **172**, 6 (2017).
25. Schmälzlin E., Moralejo B., Bodenmüller D., Darvin M.E., Thiede G., Roth M.M. *J. Sens. Sens. Syst.*, **5**, 261 (2016).
26. Schmälzlin E., Moralejo B., Gersonde I., Schleusener J., Darvin M.E., Thiede G., Roth M.M. *J. Biomed. Opt.*, **23**, 105001 (2018).
27. Darvin M.E., Schleusener J., Parenz F., Seidel O., Krafft C., Popp J., Lademann J. *Analyst*, **143**, 4990 (2018).
28. Franzen L., Selzer D., Fluhr J.W., Schaefer U.F., Windbergs M. *Eur. J. Pharmaceut. Biopharmaceut.*, **84**, 437 (2013).
29. Miloudi L., Bonnier F., Barreau K., Bertrand D., Perse X., Yvergnaux F., Byrne H.J., Chourpa I., Munnier E. *Analyst*, **143**, 2377 (2018).
30. Zhang G., Moore D.J., Flach C.R., Mendelsohn R. *Anal. Bioanal. Chem.*, **387**, 1591 (2007).
31. Tsai T.-H., Short M.A., McLean D.I., Zeng H., McElwee K., Lui H. *Analyst*, **139**, 2799 (2014).
32. Franzen L., Mathes C., Hansen S., Windbergs M. *J. Biomed. Opt.*, **18**, 061210 (2013).
33. Valiveti S., Wesley J., Lu G.W. *Int. J. Pharm.*, **346**, 10 (2008).
34. Pfannes E.K.B., Weiss L., Hadam S., Gonnet J., Combardiere B., Blume-Peytavi U., Vogt A. *Skin Pharmacol. Physiol.*, **31**, 115 (2018).
35. Zhang L., Henson M.J., Sekulic S.S. *Anal. Chim. Acta*, **545**, 262 (2005).
36. Vajna B., Farkas I., Szabo A., Zsigmond Z., Marosi G. *J. Pharm. Biomed. Anal.*, **51**, 30 (2010).
37. Miloudi L., Bonnier F., Tfayli A., Yvergnaux F., Byrne H.J., Chourpa I., Munnier E.J. *Biophotonics*, **11**, e201700221 (2018).
38. Caspers P.J., Lucassen G.W., Carter E.A., Bruining H.A., Puppels G.J. *J. Investigat. Dermatol.*, **116**, 434 (2001).
39. Ragno G., Vetuschi C., Risoli A., Ioele G. *Talanta*, **59**, 375 (2003).
40. Jaumot J., de Juan A., Tauler R. *Chemometr. Intellig. Lab Syst.*, **140**, 1 (2015).
41. Felten J., Hall H., Jaumot J., Tauler R., de Juan A., Gorzsas A. *Nature Protocols*, **10**, 217 (2015).
42. Colares C.J.G., Pastore T.C.M., Coradin V.T.R., Camargos J.A.A., Moreira A.C.O., Rubim J.C., Braga J.W.B. *J. Brazil. Chem. Soc.*, **26**, 1297 (2015).
43. Bonnist E.Y.M., Gorce J.P., Mackay C., Pendlington R.U., Pudney P.D.A. *Skin Pharmacol. Physiol.*, **24**, 274 (2011).
44. Veselinović A.M., Nikolić R.S., Nikolić G.M. *Central Eur. J. Chem.*, **10**, 1942 (2012).

45. Tres F., Treacher K., Booth J., Hughes L.P., Wren S.A., Aylott J.W., Burley J.C. *J. Control. Rel.*, **188**, 53 (2014).
46. Ando M., Hamaguchi H.O. *J. Biomed. Opt.*, **19**, 011016 (2014).
47. Noothalapati H., Sasaki T., Kaino T., Kawamukai M., Hamaguchi H.-O., Yamamoto T. *Sci. Rep*., **6**, 27789 (2016).
48. Feng X., Moy A.J., Nguyen H.T.M., Zhang J., Fox M.C., Sebastian K.R., Reichenberg J.S., Markey M.K., Tunnell J.W. *Biomed. Opt. Express*, **8**, 2835 (2017).
49. Tauler R. *Chemometr. Intellig. Lab. Syst*., **30**, 133 (1995).
50. Lust A., Strachan C.J., Veski P., Aaltonen J., Heinämäki J., Yliruusi J., Kogermann K. *Intern. J. Pharm*., **486**, 306 (2015).
51. Garrido M., Rius F.X., Larrechi M.S. *Anal. Bioanal. Chem.*, **390**, 2059 (2008).
52. Windig W., Guilment J. *Anal. Chem*., **63**, 1425 (1991).
53. Jacobi U., Kaiser M., Toll R., Mangelsdorf S., Audring H., Otberg N., Sterry W., Lademann J. *Skin. Res. Technol*., **13**, 19 (2007).
54. Choe C., Lademann J., Darvin M.E. *Skin Pharmacol. Physiol*., **28**, 318 (2015).
55. Galaktionov I.V., Kudryashov A.V., Sheldakova Yu.V., Byalko A.A., Borsoni G. *Quantum Electron*., **47**, 32 (2017) [*Kvantovaya Elektron*., **47**, 32 (2017)].
56. Barun V.V., Ivanov A.P. *Quantum Electron*., **47**, 371 (2017) [*Kvantovaya Elektron.*, **47**, 371 (2017)].
57. Schleusener J., Carrer V., Patzelt A., Lademann J., Darvin M.E. *Laser Phys. Lett*., **14**, 125601 (2017).
58. 2013 R: A Language and Environment for Statistical Computing Vol. 3. (Vienna, Austria); https://www.R-project.org/.
59. Bocklitz T., Walter A., Hartmann K., Rosch P., Popp J. *Analytica Chim. Acta*, **704**, 47 (2011).
60. Guo S., Bocklitz T., Popp J. *Analyst*, **141**, 2396 (2016).
61. Liland K.H., Mevik B.H. *Baseline: Baseline Correction of Spectra,* R package version 1.2-1 (2015).
62. Mullen K.M. *ALS: Multivariate Curve Resolution Alternating Least Squares* (MCR-ALS), R package version 0.0.6 (2015).
63. Ilchenko O.O., Pilgun Y.V., Reynt A.S., Kutsyk A.M. *Ukr. J. Phys*., **61**, 519 (2016).
64. Mercer E.H. *The Biology of Hair Growth* (USA, New York: Acad. Press, 1958) p. 113.
65. Voloshina O.V., Shirshin E.A., Lademann J., Fadeev V.V., Darvin M.E. *Indoor Air*, **27**, 377 (2017).
66. Williams A.C., Edwards H.G.M., Barry B.W. *J. Raman Spectrosc.*, **25**, 95 (1994).
67. Stone N., Kendall C., Smith J., Crow P., Barr H. *Faraday Discuss*., **126**, 141 (2004).
68. Frushour B.G., Koenig J.L. *Biopolymers*, **14**, 649 (1975).
69. Silveira L. Jr, Silveira F.L., Bodanese B., Zangaro R.A., Pacheco M.T.T. *J. Diomed. Opt.*, **17**, 077003 (2012).
70. Shirshin E.A., Gurfinkel Y.I., Priezzhev A.V., Fadeev V.V., Lademann J., Darvin M.E. *Sci. Rep*., **7**, 1171 (2017).
71. Czekalla C., Schonborn K.H., Doge N., Jung S., Darvin M.E., Lademann J., Meinke M.C. *Skin Pharmacol. Physiol*., **30**, 260 (2017).
72. Sdobnov A.Y., Tuchin V.V., Lademann J., Darvin M.E. *J. Phys. D: Appl. Phys*., **50**, 285401 (2017).
73. Genina E.A., Ksenofontova N.S., Bashkatov A.N., Terentyuk G.S., Tuchin V.V. *Quantum Electron*., **47**, 561 (2017) [*Kvantovaya Elektron*., **47**, 561 (2017)].
74. Blume-Peytavi U., Vogt A. *Br. J. Dermatol*., **165**, Suppl. 2, 13 (2011).